Molecular Biology of the Cell
Vol. 6, 1591–1603, November 1995

Structural Analysis of the p62 Complex, an Assembly of *O*-linked Glycoproteins that Localizes Near the Central Gated Channel of the Nuclear Pore Complex

Tinglu Guan,* Shirley Müller,† George Klier,* Nelly Panté,† Jonathan M. Blevitt,*‡ Markus Haner,† Bryce Paschal,* Ueli Aebi,† and Larry Gerace*§

*Departments of Cell and Molecular Biology, The Scripps Research Institute, La Jolla, California 92037; and †Maurice E. Muller Institute at the Biozentrum, University of Basel, Basel, CH-4056 Switzerland

Submitted June 20, 1995; Accepted August 28, 1995
Monitoring Editor: Keith R. Yamamoto

The p62 complex is an oligomeric assembly of *O*-linked glycoproteins of the nuclear pore complex that interacts with cytosolic transport factors and is part of the machinery for nuclear protein import. In this study we have purified the p62 complex from rat liver nuclear envelopes and analyzed its structure and composition. The p62 complex consists of four distinct polypeptides (p62, p58, p54, and p45) and has a mass of ~234 kDa, calculated from its hydrodynamic properties and supported by chemical cross-linking and scanning transmission electron microscopy. These data suggest that the p62 complex contains one copy of each constituent polypeptide. Analysis of preparations of the p62 complex by electron microscopy using rotary metal shadowing and negative staining revealed donut-shaped particles with a diameter of ~15 nm. Immunogold electron microscopy of isolated rat liver nuclear envelopes demonstrated that p62 occurs on both the nucleoplasmic and cytoplasmic sides of the pore complex near the central gated channel involved in active transport of proteins and RNAs. The properties and localization of the p62 complex suggest that it may be involved in binding transport ligands near the center of the nuclear pore complex and in subsequently transferring them to the gated transport channel.

INTRODUCTION

Nucleocytoplasmic transport is mediated by nuclear pore complexes (NPCs), large supramolecular protein assemblies that span the double membrane of the nuclear envelope (NE) (Fabre and Hurt, 1994; reviewed by Panté and Aebi, 1993; Melchior and Gerace, 1995). The NPC is involved in two mechanistically distinct types of molecular transport. Small molecules cross the NPC by passive diffusion through aqueous channels with a functional diameter of ~10 nm (Peters, 1986). Most proteins and RNAs are too large to diffuse through these channels at significant rates, and instead are actively transported through a gated channel by temperature and ATP-dependent mechanisms (Newmeyer and Forbes, 1988; Richardson *et al.*, 1988) that involve specific signals on the transported molecules.

Nuclear protein import is the best characterized nucleocytoplasmic transport pathway. It is specified by nuclear localization sequences (NLSs) in the transported proteins, which are usually short stretches of amino acids enriched in basic residues (Dingwall and Laskey, 1991). NLS-mediated nuclear import is a multistep process (Newmeyer and Forbes, 1988; Richardson *et al.*, 1988). An early step is thought to involve interaction between an NLS-containing ligand and an

‡ Present address: R.W. Johnson, PRI, Assay Development, 3535 General Atomic Ct., Suite 100, San Diego, California 92121.
§ Corresponding author: The Scripps Research Institute, Department of Cell Biology, 10666 North Torrey Pines Road, La Jolla, CA 92037.

© 1995 by The American Society for Cell Biology

NLS receptor in the cytoplasm (Adam and Gerace, 1991). Subsequent steps are believed to involve association of the ligand-receptor complex with peripheral cytoplasmic regions of the NPC, movement of this transport complex to more internal regions of the NPC, and translocation through a gated central channel into the nuclear interior (Melchior and Gerace, 1995). Nuclear protein import involves multiple cytosolic factors including the NLS receptor (reviewed by Melchior and Gerace, 1995), but functional roles of these cytosolic components are still poorly understood.

Overall, the NPC has dimensions of ~120 nm × ~80 nm and an estimated mass of ~125 × 10^6 Da (Reichelt *et al.*, 1990). Three-dimensional reconstruction studies indicate that the framework of the NPC consists of a central multidomain "spoke" complex sandwiched between peripheral "rings" (Hinshaw *et al.*, 1992; Akey and Radermacher, 1993). This framework has eightfold rotational symmetry about an axis perpendicular to the nuclear surface, and twofold symmetry about an axis parallel to the nuclear surface passing through the NPC center. A central channel complex of poorly defined architecture is attached to the inside of the spokes and contains a gated channel for signal-mediated transport of macromolecules. Associated with the ring-spoke framework are sets of eight fibrils emanating from the cytoplasmic and nucleoplasmic rings (Jarnik and Aebi, 1991). In preparations of isolated amphibian NEs, the cytoplasmic fibrils are ~25–50 nm long, whereas the nucleoplasmic fibrils are 75–100 nm long and joined in a "terminal" ring at their distal ends to form a "nuclear basket" (discussed by Panté and Aebi, 1993).

The NPC is expected to consist of over 100 different polypeptides, but only a small number of these have been identified (see Fabre and Hurt, 1994). Mammalian NPCs contain a group of at least eight polypeptides modified with *O*-linked *N*-acetylglycosamine (Davis and Blobel, 1987; Snow *et al.*, 1987), which contain multiple copies of degenerate FG-containing repeats. A transport role for at least some of the NPC *O*-linked glycoproteins has been suggested by numerous studies (reviewed by Fabre and Hurt, 1994; Melchior and Gerace, 1995). The most extensively analyzed *O*-linked glycoprotein is p62, which contains at least 10 mol of *O*-linked *N*-acetylglucosamine (Holt *et al.*, 1987). The cDNA sequence has been determined for p62 from several vertebrates (Starr *et al.*, 1990; Carmo-Fonseca *et al.*, 1991; Cordes *et al.*, 1991). This work indicates that the protein contains two prominent domains, an amino terminal region (residues 1–324 in rat p62) with 15 or more degenerate repeats of the form GFXFG, and a carboxyl terminal region (residues 325–523 in rat p62) with three ~30–40 amino acid segments that have a high probability of forming α-helical coiled-coils. Previous biochemical studies of solubilized NPC proteins have indicated that p62 is stably associated with at least two other *O*-linked glycoproteins, p58 and p54, to form a "p62 complex" (Finlay *et al.*, 1991; Kita *et al.*, 1993). Interest has recently focused on p62 because it has been shown to interact with the cytosolic nuclear transport factor NTF2 (Paschal and Gerace, 1995), and thus appears to directly participate in nuclear protein import.

Understanding the mechanisms of nuclear protein import will require determination of the structure of the NPC at high resolution. With 3-D reconstruction techniques, it has been possible to map the structure of the NPC to a resolution of 5–10 nm (Hinshaw *et al.*, 1992; Akey and Radermacher, 1993). However, the size and lability of this complex makes higher resolution difficult to achieve. A complementary approach involves the imaging of isolated substructures of the NPC at high resolution, and incorporation of this information into the 3-D map of the NPC. As a first step toward this goal, we have isolated the p62 complex from rat liver NEs and analyzed its structure by biochemical and electron microscopic techniques. We found that the rat p62 complex contains four *O*-linked glycoproteins, p62, p58, p54, and p45 and has a mass of ~234 kDa. Electron microscopy of preparations of the p62 complex revealed donut-shaped particles with a diameter of ~15 nm. In immunogold electron microscopy of isolated rat liver NEs, we found that p62 is localized on both the cytoplasmic and nucleoplasmic sides of the NPC near the central gated channel. The properties of the p62 complex suggest an involvement in binding transport ligands in a central region of the NPC and transferring them to the gated channel.

MATERIALS AND METHODS

Antibody Production

Production of the RL1 monoclonal IgM, which reacts with at least eight *O*-linked glycoproteins of the NPC, has been described previously (Snow *et al.*, 1987). The RL31 hybridoma line, which secretes an IgG that reacts with p62, was obtained by immunizing an Armenian hamster with an *O*-linked glycoprotein-enriched fraction from rat liver NEs, and fusing the spleen cells of this animal with a mouse myeloma cell line as described (Snow *et al.*, 1987). For isolation of RL31 antibodies, hybridoma cells were grown in ExCell 300 serum-free medium (JRH Bioscience, Lenaxa, KS) supplemented with penicillin/streptomycin. The culture medium was collected by centrifugation in a Beckman J6B centrifuge (Beckman Instruments, Fullerton, CA) at 4000 rpm for 30 min. Solid ammonium sulfate was gradually added to yield a 50% saturated solution, and the solution was slowly stirred for 6 h at 4°C. The precipitate was then collected by centrifugation, and the pellet was resuspended in phosphate-buffered saline (PBS) and dialyzed against PBS overnight. The concentrated antibody was further purified by binding to a protein G column (Pharmacia Biotech, Piscataway, NJ) and eluting with 0.1 M glycine-HCl, pH 2.7. The protein G eluate was neutralized with 2 M Tris-HCl, pH 8.8, and was dialyzed against PBS overnight and concentrated with a colloidion membrane apparatus (Shleicher & Schuell, Keene, NH).

Polyclonal antibodies against p62 were produced by the immunization of rabbits with individual *O*-linked glycoprotein bands, which were obtained by immunoadsorption from solubilized rat liver NEs with the RL1 monoclonal antibody followed by SDS gel electrophoresis (Snow *et al.*, 1987). Monospecific anti-p62 antibodies were affinity-purified using the p62 band that was excised from a nitrocellulose transfer of an SDS gel of WGA (wheat germ agglutinin) binding proteins from rat liver NEs. The blot strip was preblocked with 10% bovine serum albumin (BSA) in PBS and then incubated with diluted antiserum overnight. The antibody was then eluted with 0.1 M sodium acetate, pH 4.5, dialyzed against PBS overnight, and concentrated with a colloidion membrane apparatus (see above).

Purification of the p62 Complex

Nuclei and NEs were isolated from rat liver as described previously (Gerace *et al.*, 1984). 600-3000 ODs of NE (1 OD is the amount derived from 3×10^6 nuclei) were solubilized by incubation for 1 h at 4°C at a concentration of 200 OD/ml in 20 mM *N*-2-hydroxyethylpiperazine-*N'*-2-ethanesulfonic acid (HEPES)-NaOH, pH 7.4, 2% *N*-octylglucoside, 600 mM NaCl, 1 mM $MgCl_2$, 1 mM dithiothreitol, 1 mM phenylmethylsulfonyl fluoride, and 1 μg/ml leupeptin. The solution was centrifuged at 45,000 rpm for 20 min in a Beckman 70.1Ti rotor, and the supernatant was mixed with WGA-Sepharose beads (Sigma, St. Louis, MO) at 400 0D/50 μl packed beads for 2 h at 4°C. The beads were then washed with 20 mM HEPES, pH 7.4, 0.1% *N*-octylglucoside, 250 mM NaCl, 1 mM $MgCl_2$, 1 mM phenylmethylsulfonyl fluoride, and eluted by incubating with 20 mM HEPES, pH 7.4, 0.5% *N*-octylglucoside, 1 M *N*-acetylglycosamine, 250 mM NaCl, 1 mM MgCl (125 μl beads/300 μl elution buffer) for 0.5–1.5 h. The eluate was centrifuged at 65,000 rpm for 20 min in a Beckman TLA 100.2 rotor, and the supernatant was chromatographed on a Superose 6 column (Pharmacia Biotech, Piscataway, NJ), which had been pre-equilibrated with 20 mM HEPES, pH 7.4, 0.1% *N*-octylglucoside, 250 mM NaCl, 1 mM $MgCl_2$, and 1 μg/ml leupeptin. The peak fractions containing the p62 complex, as determined by immunoblotting or A_{280}, were pooled and stored on ice until analysis. The Stokes radius of the p62 complex was determined by comparing its elution position from the Superose 6 column with a set of gel filtration standards (Bio-Rad Laboratories, Hercules, CA), consisting of thyroglobulin, IgG, ovalbumin, myoglobin, and vitamin B12. From 1000 OD of NEs, we obtained ~10–15 μg of purified p62 complex.

Biochemical Characterization of the p62 Complex

To determine the sedimentation coefficient of the p62 complex, the purified complex was centrifuged for 16 h in a Beckman SW41 rotor at 36,000 rpm on a 5–20% sucrose gradient containing 20 mM HEPES, pH 7.4, 0.1% *N*-octylglucoside, 250 mM NaCl, 1 mM $MgCl_2$, 1 μg/ml leupeptin. A total of 18 fractions were collected and analyzed by SDS-PAGE, either with silver staining or immunoblotting with RL1. Sedimentation standards were thyroglobulin (19 S), catalase (11.2 S), IgG (7 S), and β-lactoglobulin (2.8 S). The peak containing the p62 complex was prepared for electron microscopy as described below. In some experiments, we analyzed the total solubilized NE proteins by sucrose gradient centrifugation. The sedimentation coefficient defined for the particle containing p62, p58, p54, and p45 in this crude fraction was identical to that for the purified p62 complex.

The purified p62 complex was also analyzed by chemical cross-linking with glutaraldehyde. After adding glutaraldehyde to final concentrations of 0.02–0.2% to the purified p62 complex, the solution was incubated for 30 min on ice. SDS gel sample buffer (Gerace *et al.*, 1982) was then added to the cross-linking mixture, and the mixture was analyzed by SDS-PAGE.

SDS-PAGE was carried out as described (Gerace *et al.*, 1982). Proteins were visualized by Coomassie blue staining, silver staining (Rabilloud *et al.*, 1988), or immunoblotting with RL1 (Snow *et al.*, 1987).

Electron Microscopy and Immunogold Labeling

We investigated a variety of different methods to image the p62 complex by rotary metal shadowing. Traditional glycerol spraying (e.g. Fowler and Aebi, 1983) and centrifugal spreading methods (Nave *et al.*, 1989) did not yield a well-preserved morphology of the p62 complex. The best results were obtained using a method that involved direct adsorption to a mica surface. Specifically, the purified p62 complex (~6 μg/ml) was mixed with glycerol to a final concentration of 10–40% glycerol. Five microliters of this mixture was applied to the surface of a freshly cleaved piece of mica with an area of about 1 cm^2. The sample was dried at 10^{-6}-10^{-7} torr in a Balzers BAF-400 freeze fracture device or an Edwards Turbo 306 vacuum evaporator, and the mica was then rotary shadowed at 7–10°C with either platinum or tungsten followed by carbon at 90°C. For negative staining, 2–5 μl of purified p62 complex were applied to a glow-discharged carbon-coated grid for 30–60 s, the excess solution was withdrawn with a piece of filter paper, and a drop of 2% uranyl acetate was then applied to the grid for 1 min. Excess stain was removed and the grid was air dried before visualization. For immunogold labeling, 2–5 μl of purified p62 complex were applied to a glow-discharged carbon-coated grid for 30–60 s and the excess solution was withdrawn. One drop of 3% BSA in PBS was applied to the grid, and after 5 min the grid was rinsed with PBS. The grid was then incubated for 1 h at room temperature with the primary antibody (RL1 or RL31) diluted to a concentration of ~100 μg/ml in PBS containing 1% BSA. The grid was washed with PBS, and then incubated for 1 h at room temperature with goat anti-mouse IgG conjugated with 5-nm colloidal gold (Zymed Laboratories, South San Francisco, CA) in PBS containing 0.3% BSA. In some cases, the grid was labeled with WGA conjugated to 5-nm colloidal gold (EY Laboratories, San Mateo, CA) instead of with antibodies. The grid was then washed in PBS and negatively stained as described above.

For localization of p62 in isolated rat liver NEs, unfixed NEs at a concentration of ~400 OD/ml were incubated with primary antibodies (RL31 at 5–35 μg/ml or affinity-purified rabbit anti-p62) in PBS containing 1% BSA with gentle mixing for 1 h at room temperature. Samples were then diluted with 5–10 volumes of PBS and centrifuged at 9000 rpm in an Eppendorf centrifuge to pellet the NEs. Next, samples were resuspended in PBS with 1% BSA, secondary antibodies conjugated with 5-nm colloidal gold (Zymed Laboratories) were added, and samples were incubated for 1 h at room temperature. Samples were then diluted with 5–10 volumes of PBS and the NEs were pelleted as above. These pellets were fixed with 2% glutaraldehyde containing 0.05% tannic acid in PBS for 0.5 h at room temperature. After washing with PBS, the pellets were post-fixed with 1% osmium tetroxide in PBS for 1 h. Finally, samples were dehydrated and embedded in Epon 812 resin as described (Snow *et al.*, 1987). Sections were stained with 2% uranyl acetate for 1 min or 4% lead citrate for 7–10 min. Micrographs were recorded with a Hitachi 600 electron microscope (San Jose, CA) at 80 kV.

Scanning Transmission Electron Microscopy (STEM) Mass Measurements

2.5-μl drops of native p62 complex preparations (0.1 mg/ml), after a 5 min fixation with 0.1% glutaraldehyde, were adsorbed for 30 s to glow-discharged EM grids (i.e., gold-coated, 400-mesh/inch copper grids) that had been covered with a thin (2.5 nm) carbon film supported by a fenestrated thick carbon layer. After blotting off excess liquid, the grids were washed on at least four 100-μl droplets of quartz bi-distilled water before they were freeze dried in the microscope (Engel and Meyer, 1980). The Vacuum Generators (East Grinstead, UK) STEM HB-5 used had been calibrated for mass analysis (Müller *et al.*, 1992). Low dose, 512 × 512-pixel digital

images were recorded at 80 kV accelerating voltage and a nominal magnification of 200,000×. All microscope parameters, including the exact magnification and dose for each image, were recorded. The evaluation was carried out as described previously (Müller *et al.*, 1992). The behavior of protein particles of similar mass was assumed for the required mass loss corrections: $y = 100 - 0.029\times$ for the range below 400 kDa [selenocysteine synthase (Müller *et al.*, 1992)], $y = 100 - 0.013\times$ for the range around 800 kDa (GroEL; our unpublished results), and $y = 100 - 0.010\times$ for the range around 1000 kDa [thermosomes of *Thermoplasma acidophilum* (Waldmann *et al.*, 1995)], where y is the residual mass in % and × is the irradiation dose in e^-/nm^2.

RESULTS

Isolation and Biochemical Characterization of the p62 Complex from Rat Liver Nuclear Envelopes

We utilized a rapid two-step procedure to purify the p62 complex from rat liver NEs using WGA affinity chromatography followed by molecular sieving. Fractionation was monitored by immunoblotting with RL1 (Snow *et al.*, 1987), a monoclonal antibody that reacts with eight *O*-linked glycoproteins of rat liver NEs, including the four polypeptides found in the p62 complex (p62, p58, p54, and p45; see below). It should be noted that individual *O*-linked glycoproteins are labeled to different relative intensities by RL1, depending on the amount of total protein on the immunoblot and the exact blotting conditions (Snow *et al.*, 1987), so the intensity of staining by RL1 does not necessarily reflect the relative stoichiometries of different *O*-linked proteins in a particular sample.

NEs (Figure 1A, lane 1) were initially incubated with a solution containing 2% octylglucoside and 0.6 M NaCl. This treatment efficiently solubilized the 45- to 62-kDa *O*-linked glycoproteins, but incompletely extracted the high molecular mass glycoproteins (Figure 1A, lanes 2 and 3). All of the solubilized glycoproteins bound to WGA-Sepharose, but under our conditions mainly p62, p58, p54, and p45 were eluted with competing *N*-acetylglucosamine (Figure 1A, lanes 4 and 5). This eluted material was then fractionated on a Superose 6 gel filtration column. The 62-, 58-, 54-, and 45-kDa polypeptides all coeluted in a roughly symmetrical peak with a Stokes radius of 8.1 nm (Figure 1B, lanes 1–7; Table 1). The pooled peak fractions, which constitute the purified p62 complex, contain p62, p58, p54, and p45 and show no significant level of contamination with other proteins, as shown by Coomassie blue staining (Figure 1B, lane 8).

Although p58 and p54 have been found to copurify with p62 in previous studies (Finlay *et al.*, 1991; Kita *et al.*, 1993; Buss and Stewart, 1995), a cofractionating 45-kDa polypeptide has been seen in only some preparations (Kita *et al.*, 1993). This could be explained by p45 being selectively protease-sensitive compared with the other three polypeptides of the p62 complex. Consistent with this, in our hands p45 is diminished or absent from NE preparations that have undergone overt proteolysis as indicated by the loss of high molecular mass RL1-reactive bands and the appearance of additional RL1-reactive bands in the 45- to 62-kDa range (our unpublished observations). We have no evidence that p45 itself is generated by in vitro proteolysis as previously proposed by others (Kita *et al.*, 1993). The p45 band clearly is not proteolytically generated during the nuclease digestion steps used for the isolation of NEs from nuclei, because p45 is prominent in a WGA-binding fraction isolated from unfractionated rat liver nuclei (Figure 1A, lane 6).

The bands corresponding to p62, p58, and p54 have similar Coomassie blue staining intensities in the purified complex, while p45 is less intensely stained (Fig-

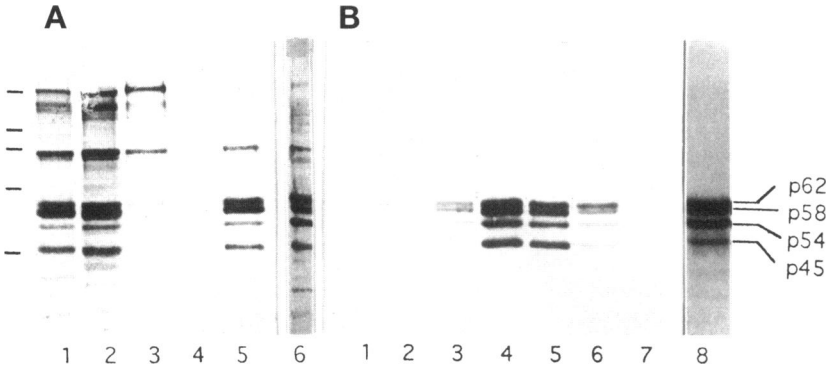

Figure 1. Purification of the p62 complex from rat liver nuclear envelopes. (A) Isolated rat liver NEs (lane 1) were extracted with *N*-octylglucoside and sedimented to yield a supernatant (lane 2) and a pellet (lane 3). The supernatant was applied to WGA-Sepharose beads. The unbound fraction (lane 4) and a fraction eluted with *N*-acetylglucosamine (lane 5) were collected. In a separate experiment, WGA-binding proteins from isolated rat liver nuclei were isolated by WGA-Sepharose chromatography (lane 6). The various fractions were electrophoresed on a 10% SDS gel and visualized by immunoblotting with the RL1 monoclonal antibody, which reacts with eight *O*-linked glycoproteins of NEs. The OD equivalents (see MATERIALS AND METHODS) analyzed are as follows: lanes 1–3, 10 OD; and lanes 4–6, 20 OD. (B) Purified WGA-binding proteins isolated from rat liver NEs (lane 5 of panel A) were chromatographed on a Superose 6 molecular sieving column. Shown is an immunoblot of the column fractions eluting near the peak of the p62 complex (lanes 1–7), electrophoresed on a 8% SDS gel, and probed with RL1. The peak fractions from the Superose 6 column containing the p62 complex were pooled and stained with Coomassie blue after electrophoresis (lane 8). The OD equivalents analyzed are as follows: lanes 1–7, 200 OD; and lane 8, 100 OD. Lines to the left of panel A indicate migrations of the molecular mass markers: 205 kDa, 117 kDa, 97 kDa, 66 kDa, and 45 kDa. The migrations of p62, p58, p54, and p45 are indicated at the right of panel B.

ure 1B, lane 8). However, because of the nonuniform staining properties of different proteins, it is not possible to determine the relative stoichiometry of these components accurately using protein staining.

When the purified p62 complex was analyzed by sucrose gradient centrifugation, p62, p58, p54, and p45 all cosedimented (our unpublished observations) as reported previously (Kita *et al.*, 1993). We found the purified p62 complex as well as the p62 complex released in a crude supernatant by NE solubilization (as in Figure 1A, lane 2) to have a sedimentation coefficient of 7 S by this procedure (Table 1). Assuming that the p62 complex has a partial specific volume of 0.73, we calculated its molecular mass to be 234 kDa (Table 1). The complex has a frictional ratio of 1.8 (Table 1), indicating that it is somewhat asymmetric in shape.

We further analyzed the mass of the p62 complex by chemical cross-linking (Figure 2). When the purified complex was cross-linked with increasing concentrations of glutaraldehyde from 0.02–0.2%, all four monomeric polypeptides disappeared, and in their place appeared a prominent RL1-reactive band migrating with an apparent mass of about 200 kDa (Figure 2A, lanes 1–5). If the sample was treated with 1% SDS to dissociate the subunits before treatment with glutaraldehye, the 200-kDa band was not obtained (our unpublished observations). The glutaraldehyde cross-linking also yielded minor amounts of two bands having slower mobilities, suggesting that the p62 complex may be able to self-associate into higher order oligomers. Thus, the results of chemical cross-linking strongly support the mass of ~234 kDa calculated for the p62 complex from its hydrodynamic properties.

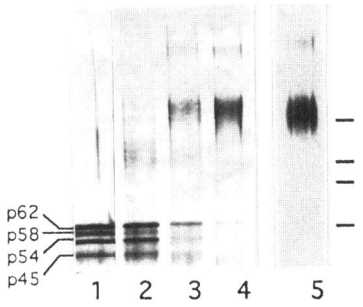

Figure 2. Analysis of the p62 complex by chemical cross-linking. The purified p62 complex was incubated with increasing concentrations of glutaraldehyde (lane 1, 0%; lane 2, 0.02%; lane 3, 0.04%; lane 4, 0.08%; and lane 5, 0.2%), electrophoresed on a 5–10% SDS gel, and stained with silver (lanes 1–4) or visualized by immunoblotting with RL1 (lane 5). Lines to the right of lane 5 represent the migrations of molecular mass markers: 205 kDa, 117 kDa, 97 kDa, and 66 kDa.

Structure of the p62 Complex

We examined preparations of the isolated p62 complex by electron microscopy after low-angle rotary metal shadowing and negative staining (Figure 3). We found p62 particles to be unusually labile structurally, as it was very difficult to obtain preparations revealing a well-preserved morphology (as indicated by fields of particles with a uniform appearance). Of several preparative methods evaluated to obtain rotary metal shadowed images, we achieved the best results by directly applying specimens to mica surfaces in a glycerol-containing solution (see MATERIALS AND METHODS). In samples of purified protein (e.g. Figure 1B, lane 8) that were rotary shadowed with platinum, grid areas with well-preserved structures contained round particles with an average diameter of ~16 nm in projection, including an undetermined thickness of metal coat (Figure 3A). Round particles of a similar size were observed in tungsten-shadowed preparations that had been subjected to an additional purification step by selecting the 7 S peak from a glycerol gradient after WGA affinity chromatography and gel filtration (Figure 3C).

When samples of the purified p62 complex were examined by negative staining, we similarly observed round particles with an average diameter of ~15 nm in projection (Figure 3B). In favorable views, the particles exhibited a distinct stain-penetrating central region (Figure 3B, arrowheads; Figure 3D, left four panels). Infrequently, we found apparent edge-on views of the p62 particle (Figure 3D, right three panels), which indicate that it is disk or donut-shaped rather than spherical. Thus, the round appearance typically seen in projection views of the p62 particle in low-angle rotary metal shadowing and negative staining appears to reflect the fact that the particle preferentially adsorbs to grids and mica surfaces in an en face orientation.

We next analyzed preparations of p62 complex by STEM to determine the mass distribution of p62 particles (Figure 4). The procedure used for STEM sample preparation (i.e., involving freeze drying and no stain-

Table 1. Physical properties of the p62 complex

Stokes radius, a	8.1 nm
Sedimentation coefficient, S	7 S
Calculated mass, M	234 kDa
Frictional ratio, f/f_o	1.8
Approximate subunit molecular weights	62, 58, 54, and 45 kDa

$$m = \frac{6\pi\eta NaS}{1 - Vp}$$

$$f/f_o = a\left(\frac{4\pi N}{3M(V + \delta p)}\right)^{1/3}$$

η = Viscosity
N = Avogadros number
S = Sedimentation coefficient
a = Stokes radius
V = Partial specific volume, 0.73 cm^3/g
p = Density
δ = 0.2 g of solvent/g of protein

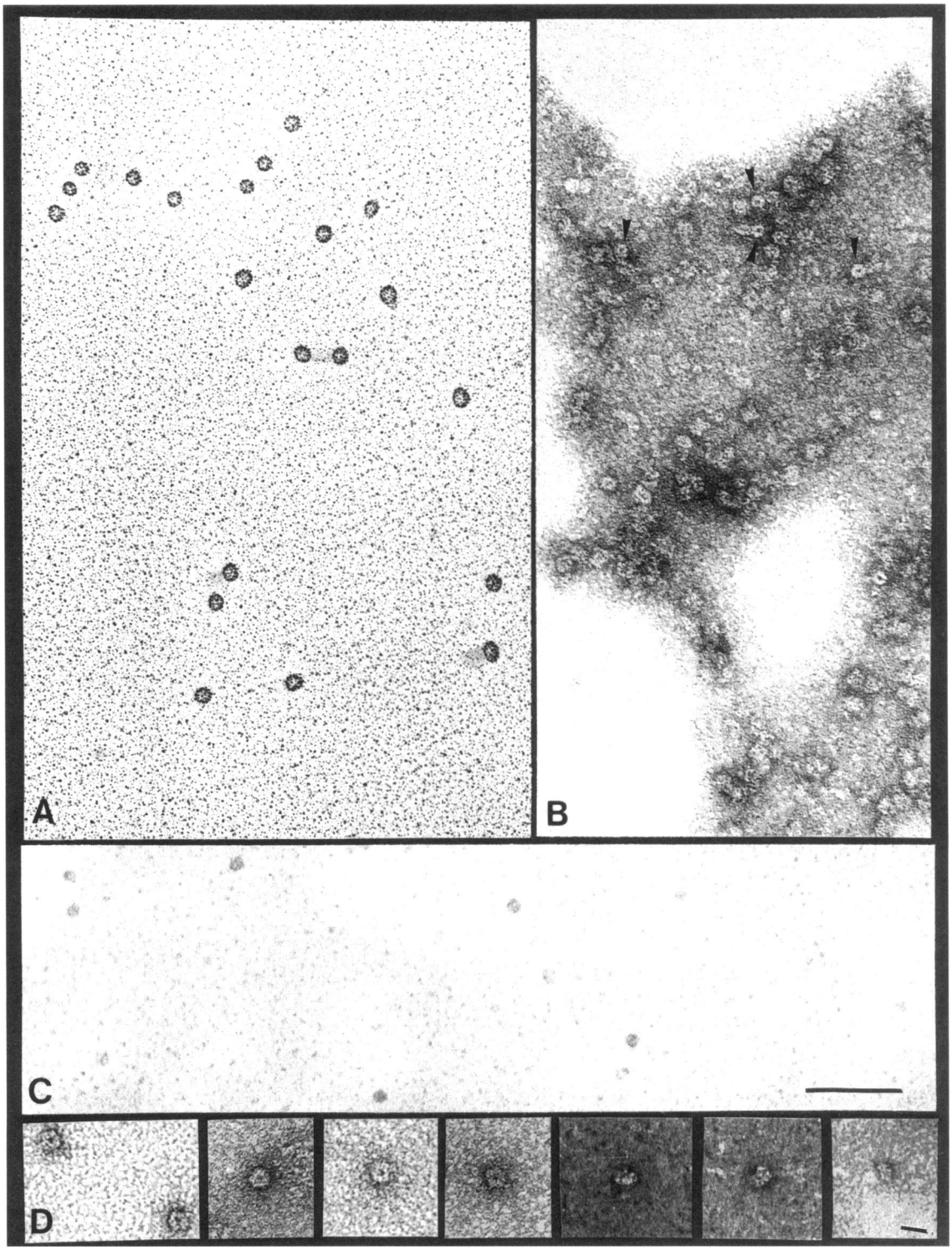

Figure 3. Imaging of the purified p62 complex by electron microscopy. Shown are electron micrographs of samples analyzed by various imaging methods. The purified p62 complex (see Figure 1, lane 8) was applied to mica and rotary shadowed with platinum (A), or was adsorbed to a grid and negatively stained with uranyl acetate (B). A sample of the purified p62 complex was further fractionated by sedimentation on a 5–20% glycerol gradient, and the peak fraction from the gradient containing the p62 complex (~7 S) was applied to mica and rotary shadowed with tungsten (C). Bar, 100 nm. (D) Gallery of selected negatively stained p62 particles in en face (left four panels) and apparent edge-on (right three panels) views. Bar, 20 nm.

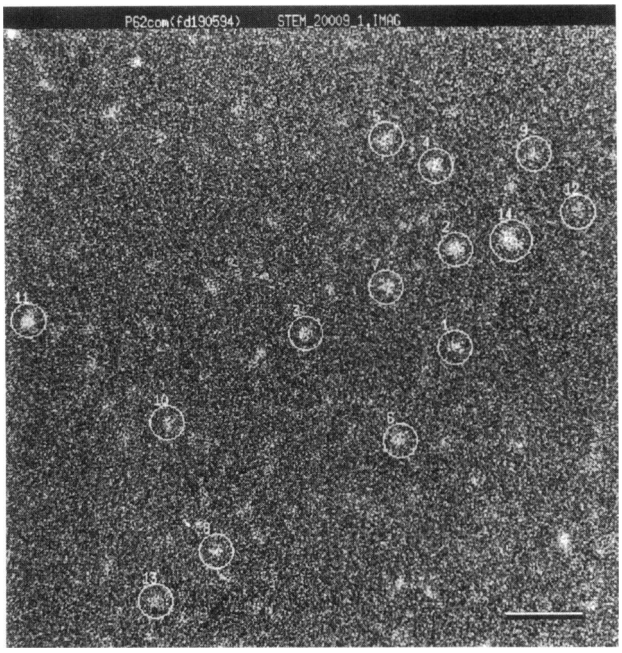

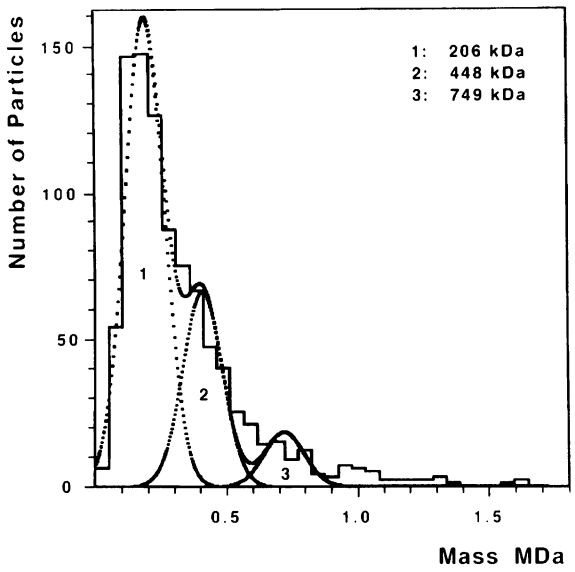

Figure 4. STEM analysis of the p62 complex. (A) Low dose STEM image of unstained/freeze-dried native p62 particles after a 5-min fixation with 0.1% glutaraldehyde. The recording dose was ~310 e-/nm^2 for this picture. Circled areas are examples of particles used for mass determination. Bar, 50 nm. (B) Mass values from unstained/freeze-dried preparations of native p62 particles after a 5-min fixation with 0.1% glutaraldehyde. Images were recorded using doses of 314 ± 22 e/nm^2. The histogram together with Gaussian fits displays the mass data from 930 particles before correction for beam-induced mass loss. The listed peak values have been corrected for beam-induced mass loss.

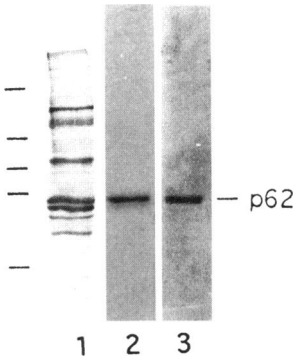

Figure 5. Characterization of antibodies used to label the p62 complex. Rat liver NEs were electrophoresed on a 8% SDS gel, and analyzed by immunoblotting with RL1 (lane 1), RL31 (lane 2), and affinity-purified polyclonal rabbit anti-p62 antibody (lane 3). Shown are the analysis of 5 OD equivalents. Both RL31 and the rabbit anti-p62 also labeled only p62 when 50 OD equivalents of WGA binding proteins were analyzed by immunoblotting (our unpublished results).

ing) did not yield fields of well-preserved donut-shaped particles as obtained with shadowing, and a somewhat heterogeneous range of particle sizes was seen (Figure 4A). Most of the particles had a mass peak of about 200 kDa (Figure 4B). However, the mass histogram had a significant shoulder extending to higher molecular weight species, which, based on Gaussian curve fitting, was consistent with a mixture of three components having masses of 206 kDa (69% of particles), 448 kDa (26% of particles), and 790 kDa (5% of particles). These data further suggest that the p62 complex may be able to self-associate into higher order oligomers, consistent with chemical cross-linking (see above).

To further characterize the p62 complex structurally, we incubated preparations of the p62 complex with various colloidal gold-coupled lectin or antibody probes (see Figure 5), and examined the specimens by negative staining (Figure 6). Samples were labeled either with WGA, the monoclonal antibody RL1 that recognizes multiple *O*-linked glycoproteins (Figure 5, lane 1), or the monoclonal antibody RL31 that is monospecific for p62 (Figure 5, lane 2). With all three labeling reagents, the gold specifically bound to the ~15-nm particles in areas near the central stain-penetrating "hole" that was revealed in unlabeled negatively stained material. The fact that virtually all gold particles were found near the center of the p62 particles imaged in these preparations further supports the notion of the p62 particle being a donut-shaped particle that preferentially adsorbs to grids in an en face orientation. The particle labeling patterns obtained with WGA and with the antibody RL1, which reacts with a sugar-containing epitope (Holt *et al.*, 1987), suggests that the *O*-linked sugars (and the RL31 epitope on p62) are concentrated at or near central regions of the p62 particle containing the hole seen in negative staining.

Localization of p62 in Rat Liver Nuclear Envelopes

Thus far, it has been controversial whether p62 is localized on both cytoplasmic and nucleoplasmic sides of the NPC, or only on one side (Dabauvalle *et*

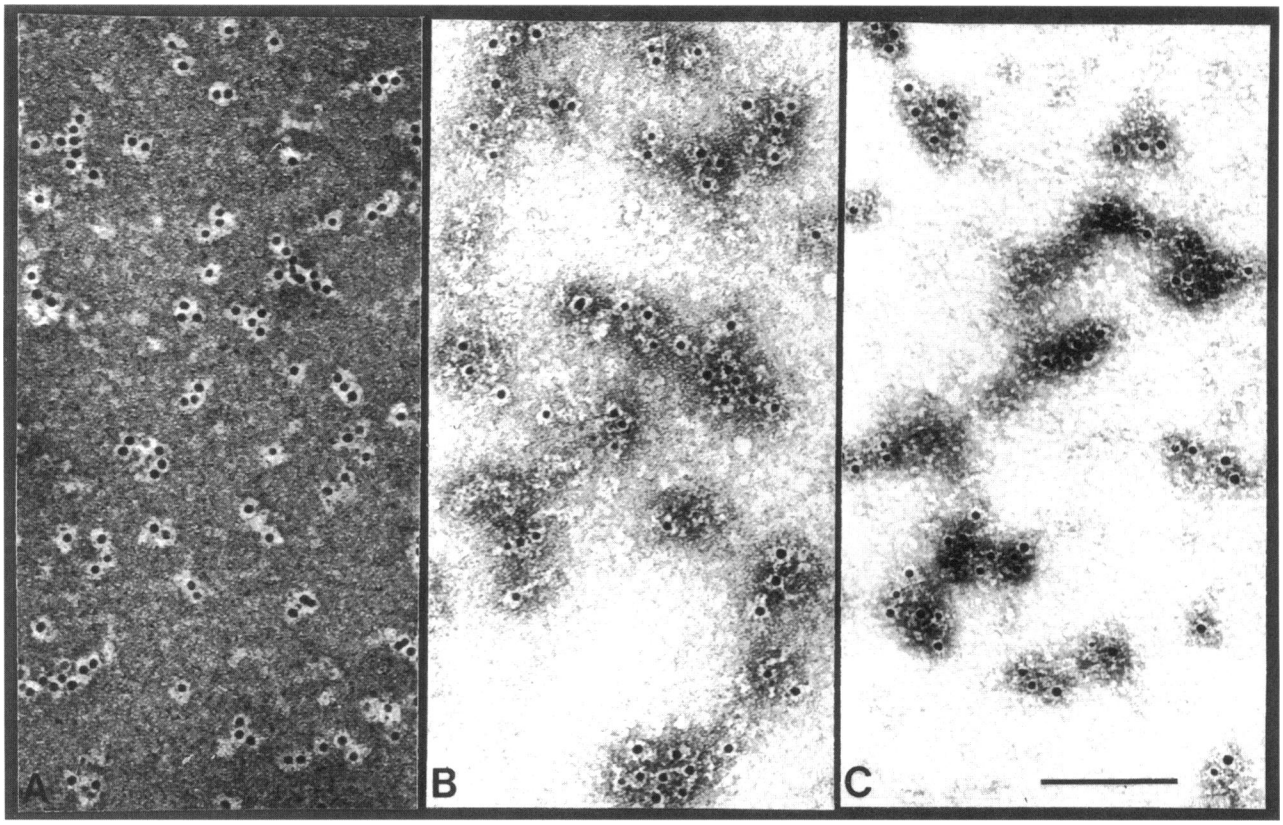

Figure 6. Immunogold labeling of the isolated p62 complex. The purified p62 complex was adsorbed to carbon-filmed grids, and incubated with WGA coupled to 5 nm gold (A), or with RL1 (B) or RL31 (C) followed by goat anti-mouse or goat anti-rabbit IgG coupled to 5 nm gold. Omission of the primary antibodies in panels B and C yielded no gold labeling of the specimens (our unpublished results). Bar, 100 nm.

al., 1988; Cordes *et al.*, 1991). To resolve this issue, and to map the localization of p62 within the NPC in detail, we carried out pre-embedding immunogold localization of p62 in isolated rat liver NEs and quantitative analysis of the distribution of gold particles. For this purpose, we used two different antibodies, both of which were monospecific for p62 in immunoblotting. One was the RL31 monoclonal antibody (Figure 5, lane 2), and the other was an affinity-purified rabbit polyclonal antibody raised against electrophoretically purified p62 from rat liver (Figure 5, lane 3). Both antibodies gave similar immunogold labeling patterns (Figure 7). The antibodies strongly decorated both cytoplasmic and nucleoplasmic surfaces of the NPC, as seen in cross-sections (Figure 7, A–E, G, H, and J–L). In both cross-sections and grazing sections (Figure 7, F, I, and M), the gold labeling was concentrated near the central channel regions of the NPC.

Quantitative analysis of the distribution of gold particles obtained by labeling with RL31 relative to the two symmetry axes of the NPC (see INTRODUCTION) is shown in Figure 8. Distances of gold particles from the eightfold symmetry axis perpendicular to the NE surface were measured in grazing sections of the NPC (e.g. Figure 7, F, I, and M), whereas distances from the central plane that divides the NPC into a nucleoplasmic and a cytoplasmic "half" were measured in cross-sections (e.g. Figure 7, A–E). Approximately 85% of the gold particles were clustered within a radius of 20 nm from the eightfold axis (Figure 8A). Thus, virtually all gold labeling occurs at a significantly smaller radius than the cytoplasmic and nucleoplasmic rings, which are seen to begin at ~31 nm from the eightfold axis in *Xenopus* oocyte NEs (Hinshaw *et al.*, 1992). In addition, almost all gold particles occurred within a distance of 30 nm from the central NPC plane, with a peak at ~20–30 nm (Figure 8B). By comparison, the cytoplasmic and nucleoplasmic "rings" occur ~30–40 nm from the central plane (Hinshaw *et al.*, 1992; Akey and Radermacher, 1993). This quantitative analysis demonstrates that p62 is concentrated near the central channel of the NPC, in contrast to the more peripheral locations found for several other *O*-linked glycoproteins (see DISCUSSION).

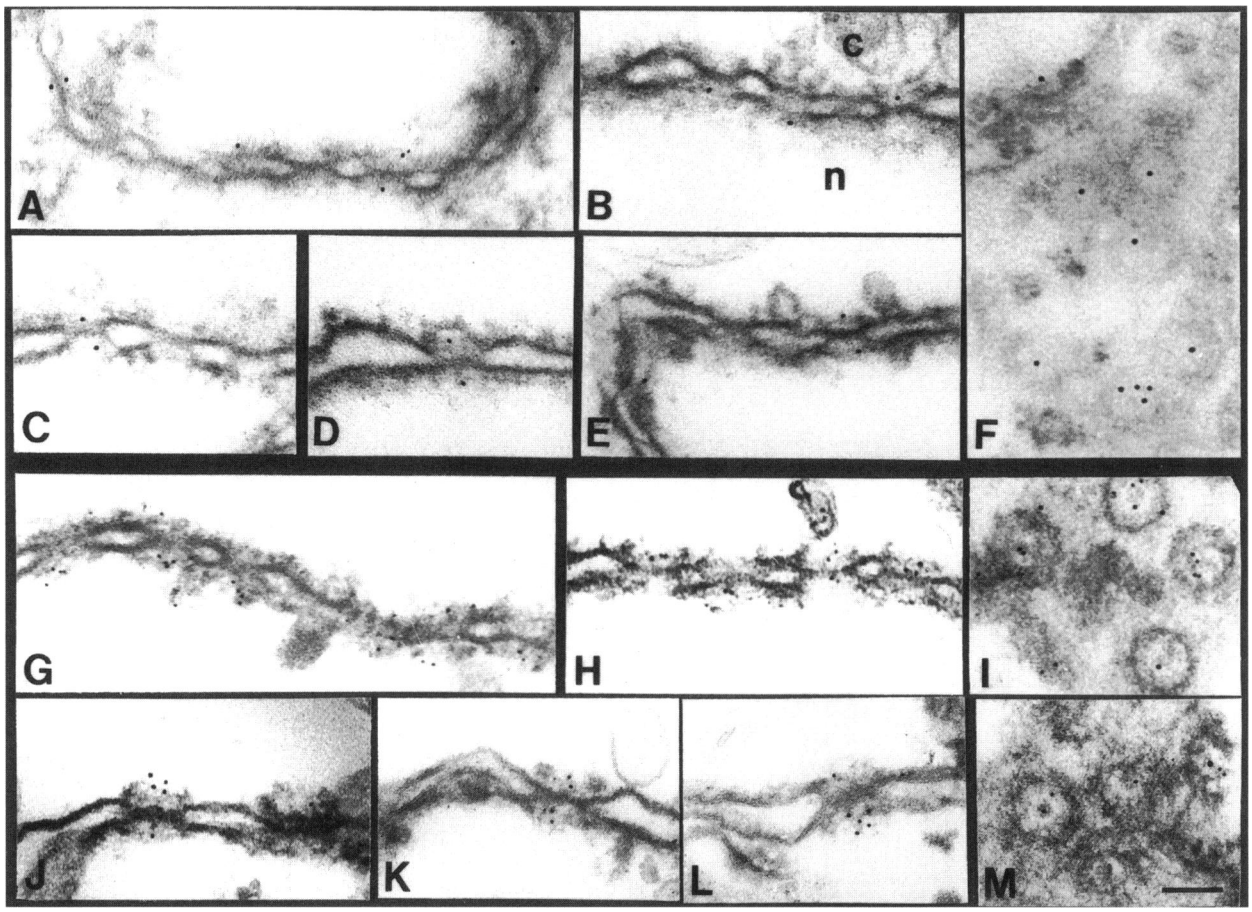

Figure 7. Immunogold localization of p62 in isolated rat liver nuclear envelopes. Isolated NEs were incubated with 5 μg/ml RL31 followed by goat anti-mouse IgG coupled to 5 nm gold (A–F) or with polyclonal rabbit anti-p62 followed by goat anti-rabbit IgG coupled to 5 nm gold (G–M). Shown are electron micrographs of thin sections showing the NE in cross-sections (A–E, G, H, and J–L) or grazing sections (F, I, and M). Omission of the primary antibodies yielded essentially no gold labeling (our unpublished results). n, nucleoplasmic surface; c, cytoplasmic surface. Bar, 100 nm.

DISCUSSION

Structure of the Isolated p62 Complex

Recent work has indicated that the p62 complex is involved in nuclear import (Finlay *et al.*, 1991) and directly interacts with at least one cytosolic transport factor (Paschal and Gerace, 1995). To help understand its functions, we have characterized the structural features of the p62 complex isolated from rat liver NEs, and have mapped the localization of p62 in situ in NPCs. The imaging of isolated substructural components of the NPC, as exemplified by our work on the p62 complex, should have widespread value for obtaining a higher resolution structural understanding of the NPC and nuclear transport mechanisms.

We found that the rat liver p62 complex contains four *O*-linked glycoproteins (p62, p58, p54, and p45) that remain stably associated in solutions containing nonionic detergent and high salt. Preparations of the rat liver p62 complex isolated by other laboratories all contain p62, p58, and p54 (Finlay *et al.*, 1991; Kita *et al.*, 1993; Buss and Stewart, 1995), but the preparations frequently lack p45. Our recent cDNA cloning (see below) indicates that p45 is a discrete cellular polypeptide and not a proteolytic product of another component. We suggest that the absence of p45 in some preparations of the p62 complex is due to its selective sensitivity to in vitro proteolysis relative to the other proteins.

Our data from three separate approaches (hydrodynamic analysis, chemical cross-linking, and STEM) all indicate that the p62 complex has a mass of ~234 kDa. This is very similar to the 231-kDa mass value for the p62 complex that was previously calculated from its hydrodynamic properties (Kita *et al.*, 1993). An earlier study involving solubilized WGA-binding proteins from rat liver NEs showed that p62, p58, and p54 are coprecipitated with antibodies to each of the individual bands (Finlay *et al.*, 1991). In this study, we have

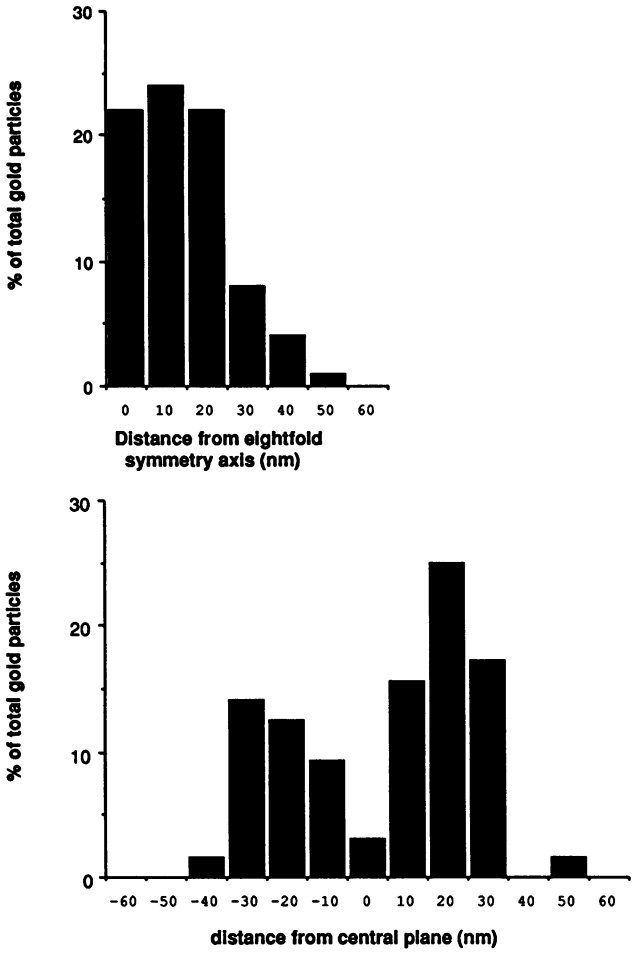

Figure 8. Quantitative analysis of gold distributions in nuclear envelopes decorated with anti-p62 antibodies. Isolated NEs were incubated with 5 μg/ml RL31 followed by goat anti-mouse IgG coupled to 5 nm gold, and electron micrographs of thin sections were recorded and printed on photographic paper. The distances of gold particles from the eightfold symmetry axis were determined from grazing sections (panel A, 87 immunogold particles scored), and the distances of gold particles from the central plane were determined from cross-sections (panel B, 74 immunogold particles scored).

demonstrated cofractionation of p62, p58, p54, and p45 by gel filtration and sucrose gradient centrifugation. The simplest model that can be deduced from this information, together with our mass data, is that the p62 complex comprises a single molecular species containing one copy of each of the four polypeptides. However, it remains possible that there are two or more nonidentical, copurifying species of the p62 complex. Our recent cDNA cloning of p58 and p45 indicates that these polypeptides are products of alternative splicing (Hu and Gerace, unpublished observations). Thus it is conceivable that some p62 complexes could contain two copies of p58 (and no p45) or two copies of p45 (and no p58) instead of a p58/p45 pair. However, as yet we have been unable to resolve complexes that differ in their p58 or p45 content by either gel filtration or sucrose gradient centrifugation. The mass we have determined for the p62 complex is incompatible with models in which the p62 complex contains two or four copies of each of the subunits (Finlay *et al.*, 1991; Buss and Stewart, 1995).

Our cDNA cloning of p58, p54, and p45 (Hu and Gerace, unpublished observations) demonstrates that the other three components of the p62 complex, like p62, also contain short stretches of heptad repeats with a high probability of forming α-helical coiled-coils. Thus, the four subunits of the p62 complex could interact by heterotypic α-helical coiled-coil interactions. In this respect, the p62 complex may be similar to a complex of NPC proteins characterized in *Saccharomyces cerevisiae* consisting of Nsp1p, Nic96p, Nup57p, and Nup49p, which are proposed to interact by coiled-coil interactions involving the four subunits (Grandi *et al.*, 1995). However, it is not known whether the yeast Nsp1 complex is functionally homologous to the mammalian p62 complex.

Analysis of preparations of the p62 complex by electron microscopy after negative staining revealed donut-shaped particles (in projection) with a diameter of ~15 nm and a distinct stain-penetrating central hole. Similarly, low-angle rotary metal shadowing of these preparations revealed round particles with a diameter of ~16 nm (including the metal coat). Apparent edge-on views in negative staining are consistent with the p62 particle being a donut-or disk-shaped rather than a spherical structure, which preferentially adsorbs to grids and mica in an en face orientation.

At the present time, we do not know whether the ~15-nm particle imaged by electron microscopy corresponds to the ~234-kDa p62 complex measured by biochemical analysis, or to a higher order oligomer of the p62 complex. Unfortunately, the preparative procedure required for STEM did not yield enough homogeneous and sufficiently well-defined ~15-nm donut-shaped particles for a direct mass assignment. The possibility that the ~15-nm particle is identical to the ~234-kDa p62 complex is consistent with the finding that ~15-nm particles were seen with preparations isolated by gel filtration (to select a peak with a Stokes radius of 8.1 nm) followed by gradient centrifugation (to select 7 S particles). Alternatively, the possibility that the ~15-nm particle is an oligomer of the ~234-kDa p62 complex is consistent with the suggestions from chemical cross-linking and STEM that the purified p62 complex may be able to self-associate. However, to accommodate the presence of fairly large fields of relatively uniform ~15-nm particles in rotary metal shadowed specimens, it would be necessary that the monomer efficiently self-assembles into an oligomeric state in the microenvironment created on the mica surface during the drying process and/or

that a putative oligomeric form of the p62 complex preferentially adsorbs to the mica surface compared with the monomeric form.

A recent study indicated that recombinant p62, expressed and purified in the absence of the other members of the p62 complex, can generate 35-nm long rod-shaped particles when visualized by rotary shadowing (Buss *et al.*, 1994). These structures differ considerably from the native p62 particles that we have imaged, where p62 is assembled in a ~15-nm diameter donut-shaped structure. This indicates that the other proteins of the p62 complex play a major role in determining the conformation of p62 in situ.

Localization of p62 In Situ

By immunogold labeling of isolated rat liver NEs with two different monospecific antibodies, we found that p62 is located on both the nucleoplasmic and cytoplasmic surfaces of the NPC. This concurs with a previous immunolocalization study involving a polyclonal antibody raised to recombinant p62 (Cordes *et al.*, 1991), but disagrees with a study involving a monoclonal antibody recognizing a carbohydrate-containing epitope found on p62 and other *O*-linked glycoproteins, which preferentially decorates the cytoplasmic surface of the NPC (Dabauvalle *et al.*, 1988). We previously estimated from Coomassie blue staining of immunoadsorbed rat liver NE protein that the NPC contains approximately eight copies of p62 (Snow *et al.*, 1987). However, this method is susceptible to inherent inaccuracies (e.g. glycoproteins often bind disproportionately low amounts of Coomassie blue). Considering this value in the context of the eightfold symmetry of the NPC and our demonstration that p62 is present on both nucleoplasmic and cytoplasmic NPC surfaces, we suggest that there may be 16 copies of the p62 complex per NPC.

The most striking finding that emerges from our present analysis is that p62 (and by inference the p62 complex) is located near the central gated channel of the NPC: the majority of gold labeling was within a radius of 20 nm of the eightfold symmetry axis, and within a distance of 30 nm from the central plane of the NPC. The localization of p62 differs markedly from that of other *O*-linked glycoproteins that have been studied, which are localized on only one side of the NPC, and at a considerably greater distance from the central NPC plane than p62. For example, Nup153 is a constituent of the nucleoplasmic fibrils (Cordes *et al.*, 1993) with several epitopes residing in the terminal ring of the nuclear basket (Panté *et al.*, 1994), which is > 100 nm from the central plane of the NPC. Furthermore, p250/CAN is associated with the cytoplasmic fibrils (Kraemer *et al.*, 1994; Panté *et al.*, 1994), which extend ~75–100 nm from the central plane. In addition, in isolated rat liver NEs processed as in the present analysis, the GTP-bound form of Ran binds to the cytoplasmic surface of the NPC at a distance of ~60 nm from the central plane (Melchior, Guan, and Gerace, unpublished observations), apparently due to interaction with the peripherally localized RanBP2 (Yokoyama *et al.*, 1995), which is an RL1-reactive glycoprotein.

Potential Functions of the p62 Complex

The localization of p62 relative to the eightfold symmetry axis of the NPC is similar to the region where nuclear import ligands accumulate near the gated channel during transport (Akey and Goldfarb, 1989). Because p62 appears to have a direct role in nuclear protein import by virtue of its interaction with at least one cytosolic transport factor (Paschal and Gerace, 1995), we propose that nuclear transport ligands, after initially binding to the cytoplasmic fibrils at the periphery of the NPC, are subsequently transferred to a "collection site" near the central channel of the NPC comprising the p62 particle (existing either as a monomeric or oligomeric form of the p62 complex; see above). The p62 particle could subsequently transfer the ligands to the central gated channel of the NPC and be part of a hypothetical transport complex that induces channel gating. To accommodate these functions, individual p62 particles could be associated with the NPC by flexible tethers, allowing them to move from a "collection" area adjacent to the eightfold axis to the central axis itself. The finding that multiple transport ligands can accumulate near the central channel of individual NPCs (Akey and Goldfarb, 1989) supports a model in which individual p62 particles displayed around the central axis act as independent ligand accumulation sites. The presence of p62 on both the nucleoplasmic and cytoplasmic surfaces of the NPC could indicate a role in nuclear export (see Dargemont *et al.*, 1995) analogous to the proposed role in nuclear import, or a role in nuclear import at both the proximal and distal sides of the gated channel.

The morphology of the p62 particle is intriguing in relation to these functional speculations. It is conceivable that the particle itself has a dynamic structure, which could expand to allow hypothetical ligand binding within its central hole, where the *O*-linked sugars appear to be concentrated. In this respect, the p62 particle could act as an adaptor that could seal one end of the gated channel during the process of ligand translocation and prevent diffusion of molecules (and/or back movement of transport ligand) through this region during mediated transport. In future studies it will be possible to investigate possible dynamic properties of the p62 particle related to interaction with cytosolic nuclear transport factors, and its potential interaction with the gated channel of the NPC.

ACKNOWLEDGMENTS

We are very grateful to Dr. K. Tokuyasu for his insightful suggestions for imaging the p62 complex, and Ken N. Goldie for recording the STEM micrographs. We thank F. Melchior, D. Sweet, S. Schmid, K. McLachlan, H. Taniura, C. Glass, F. Pirollet, K. Furukawa, and A. Saphire for comments on the manuscript and helpful discussions. We also thank M. Keeter for excellent secretarial assistance. This work was supported by grants from the National Institutes of Health (to L.G.), the Swiss National Science Foundation (to U.A.), the Human Frontier Science Program, the Lucille P. Markey Charitable Trust, the M.E. Müller Foundation of Switzerland, the Damon Runyon-Walter Winchell Cancer Fund (to B.P.), and the Department of Education of the Kanton Basel-Stadt.

REFERENCES

Adam, S.A., and Gerace, L. (1991). Cytosolic proteins that specifically bind nuclear location signals are receptors for nuclear import. Cell *66*, 837–847.

Akey, C.W., and Goldfarb, D.S. (1989). Protein import through the nuclear pore complex is a multistep process. J. Cell Biol. *109*, 971–982.

Akey, C.W., and Radermacher, M. (1993). Architecture of the *Xenopus* nuclear pore complex revealed by three-dimensional cryo-electron microscopy. J. Cell Biol. *122*, 1–19.

Buss, F., Kent, H., Stewart, M., Bailer, S.M., and Hanover, J.A. (1994). Role of different domains in the self-association of rat nucleoporin p62. J. Cell Sci. *107*, 631–638.

Buss, F., and Stewart, M. (1995). Macromolecular interactions in the nucleoporin p62 complex of rat nuclear pores: binding of nucleoporin p54 to the rod domain of p62. J. Cell Biol. *128*, 251–261.

Carmo-Fonesca, M., Kern, H., and Hurt, E.C. (1991). Human nucleoporin p62 and the essential yeast nuclear pore protein NSP1 show sequence homology and a similar domain organization. Eur. J. Cell Biol. *55*, 17–30.

Cordes, V., Waizenegger, I., and Krohne, G. (1991). Nuclear pore complex glycoprotein p62 of *Xenopus laevis* and mouse: cDNA cloning and identification of its glycosylated region. Eur. J. Cell Biol. *55*, 31–47.

Cordes, V.C., Reidenbach, S., Kohler, A., Stuurman, N., van Driel, R., and Franke, W.W. (1993). Intranuclear filaments containing a nuclear pore complex protein. J. Cell Biol. *123*, 1333–1344.

Dabauvalle, M.C., Schulz, B., Scheer, U., and Peters, R. (1988). Inhibition of nuclear accumulation of karyophilic proteins in living cells by microinjection of the lectin wheat germ agglutinin. Exp. Cell Res. *174*, 291–296.

Dargemont, C., Schmidt-Zachmann, M.S., and Kuehn, L.C. (1995). Direct interaction of nucleoporin p62 with mRNA during its export from the nucleus. J. Cell Sci. *108*, 257–263.

Davis, L.I., and Blobel, G. (1987). Nuclear pore complex contains a family of glycoproteins that includes p62: glycosylation through a previously unidentified cellular pathway. Proc. Natl. Acad. Sci. USA *84*, 7552–7556.

Dingwall, C., and Laskey, R. (1991). Nuclear targeting sequences: a consensus? Trends Biochem. Sci. *16*, 478–481.

Engel, A., and Meyer, J. (1980). Preparation of unstained protein structures for mass determination by electron scattering. J. Ultrastruct. Res. *72*, 212–222.

Fabre, E., and Hurt, E.C. (1994). Nuclear transport. Curr. Opin. Cell Biol. *6*, 335–342.

Finlay, D.R., Meier, E., Bradley, P., Horecka, J., and Forbes, D.J. (1991). A complex of nuclear pore proteins required for pore function. J. Cell Biol. *114*, 169–183.

Fowler, W.E., and Aebi, U. (1983). Preparation of single molecules and supramolecular complexes for high resolution metal shadowing. J. Ultrastruct. Res. *83*, 319–334.

Gerace, L., Comeau, C., and Benson, M. (1984). Organization and modulation of nuclear lamina structure. J. Cell Sci. Suppl. *1*, 137–160.

Gerace, L., Ottaviano, Y., and Kondor-Koch, C. (1982). Identification of a major polypeptide of the nuclear pore complex. J. Cell Biol. *95*, 826–837.

Grandi, P., Schlaich, N., Tekotte, H., and Hurt, E.C. (1995). Functional interaction of Nic96p with a core nucleoporin complex consisting of NSP1p, Nup49p and a novel protein Nup57p. EMBO J. *14*, 76–87.

Hinshaw, J.E., Carragher, B.O., and Milligan, R.A. (1992). Architecture and design of the nuclear pore complex. Cell *69*, 1133–1141.

Holt, G.D., Snow, C.M., Senior, A., Haltiwanger, R.S., and Gerace, L. (1987). Nuclear pore complex glycoproteins contain cytoplasmically disposed *O*-linked *N*-acetylglucosamine. J. Cell Biol. *104*, 1157–1164.

Jarnik, M., and Aebi, U. (1991). Toward a more complete 3-D structure of the nuclear pore complex. J. Struct. Biol. *107*, 291–308.

Kita, K., Omata, S., and Horigome, T. (1993). Purification and characterization of a nuclear pore glycoprotein complex containing p62. J. Biochem. *113*, 377–382.

Kraemer, D., Wozniak, R.W., Blobel, G., and Radu, A. (1994). The human CAN protein, a putative oncogene product associated with myeloid leukemogenesis, is a nuclear pore complex protein that faces the cytoplasm. Proc. Natl. Acad. Sci. USA *91*, 1519–1523.

Melchior, F., and Gerace, L. (1995). Mechanisms of nuclear protein import. Curr. Opin. Cell Biol. (*in press*).

Müller, S.A., Goldie, K.N., Bürki, R., Häring, R., and Engel, A. (1992). Factors influencing the precision of quantitative scanning transmission electron microscopy. Ultramicrosc. *46*, 317–334.

Nave, R., Furst, D.O., and Weber, K. (1989). Visualization of the polarity of isolated titin molecules: a single globular head on a long rod as the M band anchoring domain? J. Cell Biol. *109*, 2177–2187.

Newmeyer, D., and Forbes, D.J. (1988). Nuclear import can be separated into distinct steps in vitro: nuclear pore binding and translocation. Cell *51*, 641–653.

Panté, N., and Aebi, U. (1993). The nuclear pore complex. J. Cell Biol. *122*, 977–984.

Panté, N., Bastos, R., McMorrow, I., Burke, B., and Aebi, U. (1994). Interactions and three-dimensional localization of a group of nuclear pore complex proteins. J. Cell Biol. *126*, 603–617.

Paschal, B.M., and Gerace, L. (1995). Identification of NTF2, a cytosolic factor for nuclear import which interacts with nuclear pore complex protein p62. J. Cell Biol. *129*, 925–937.

Peters, R. (1986). Fluorescence microphotolysis to measure nucleocytoplasmic transport and intracellular mobility. Biochem. Biophys. Acta. *864*, 305–359.

Rabilloud T., Carpentier, G., and Tarroux, P. (1988). Improvement and simplification of low-background silver staining of proteins by using sodium dithionite. Electrophoresis *9*, 288–291.

Reichelt, R., Holzenburg, A., Buhle, E.L., Jr., Jarnik, M., Engel, A., and Aebi, U. (1990). Correlation between structure and mass distribution of nuclear pore complex components. J. Cell Biol. *110*, 883–894.

Richardson, W.D., Mills, A.D., Dilworth, S.M., Laskey, R.A., and Dingwall, C. (1988). Nuclear protein migration involves two steps: rapid binding at the nuclear envelope followed by slower translocation through nuclear pores. Cell *52*, 655–664.

Snow, C.M., Senior, A., and Gerace, L. (1987). Monoclonal antibodies identify a group of nuclear pore complex glycoproteins. J. Cell Biol. *104*, 1143–1156.

Starr, C.M., D'Onofrio, M., Park, M.K., and Hanover, J.A. (1990). Primary sequence and heterologous expression of nuclear pore glycoprotein p62. J. Cell Biol. *110*, 1861–1871.

Waldmann, T., Nimmesgern, E., Nitsch, M., Peters, J., Pfeifer, G., Müller, S., Kellermann, J., Engel, A., Hartl, F.U., and Baumeister, W. (1995). The thermosome of *Thermoplasma acidophilum* and its relationship to the eukaryotic chaperonin TRiC. Eur. J. Biochem. *227*, 848–856.

Yokoyama, N., Hayashi, N., Seki, T., Panté, N., Ohba, T., Nishii, K., Kuma, K., Hayashida, T., Miyata, T., Aebi, U., Fukui, M., and Nishimoto, T. (1995). RanBP2, a giant nuclear pore complex protein that has Zn^{2+}-fingers, a cyclophilin domain, and binds Ran/TC4. Nature (*in press*).